Interfacial and (emulsion) gel rheology of hydrophobised whey proteins

Ashkan Madadlou, Marie-Hélène Famelart, Stéphane Pezennec, Florence Rousseau, Juliane Floury, Didier Dupont

Interfacial and (emulsion) gel rheology of hydrophobised whey proteins

Ashkan Madadlou, Marie-Helene Famelart, Stéphane Pezennec, Florence Rousseau, Juliane Floury, Didier Dupont*

STLO, UMR 1253, INRA, Agrocampus Ouest, 35000 Rennes, France

*Corresponding author. Tel.:

E-mail address: didier.dupont@inra.fr (D. Dupont)

ABSTRACT

Hydrophobisation of whey proteins, followed by erythritol addition into the hydrophobised protein dispersion, enables formation of water-in-water (W/W) emulsions of the proteins and alginate. In this study, we investigated the interfacial and gel rheology of whey proteins as affected by hydrophobisation, heat denaturation and erythritol addition. Additionally, the gel rheology of the resultant W/W emulsion was assessed. Hydrophobisation shortened the linear viscoelastic region and decreased the surface storage modulus (G_s'), the flow stress and the flow strain of protein layer at the air-liquid interface. Erythritol addition into the hydrophobised protein caused a further reduction of G_s'. In accordance with interfacial rheology, protein hydrophobisation and erythritol addition decreased the dynamic moduli of acid-induced protein gels. Frequency sweep tests indicated that the gelled emulsion had higher dynamic moduli than all WPI gels. The higher firmness of the emulsion gel was ascribed, based on microstructural images, to micro-phase separation of alginate droplets.

1. Introduction

Different types of whey proteins, such as β-lactoglobulin (β-lg) and bovine serum albumin, as well as whey protein products such as whey protein isolate (WPI) and whey protein concentrate (WPC), are widely used in various fields of food technology, including foam and emulsion stabilisation (Jaishankar, Sharma, & McKinley, 2011), fat replacement, and gel formation (Zhang, Arrighi, Campbell, Lonchamp, & Euston, 2018). Each application may require modification of one or several functional properties of whey proteins. Enzymatic hydrolysis, heat-induced polymerisation (Foegeding, Davis, Doucet, & McGuffey, 2002), high pressure processing (Liu, Powers, Swanson, Hill, & Clark, 2005), and chemical functionalisation (Zhao, Ma, Yuen, & Phillips, 2004) are examples of whey protein modifications.

Recently, WPI was hydrophobised through a process consisting of two consecutive steps including a pre-acetylation stage followed by a combined acetylation/heat treatment period. The process resulted in acetylation of ≥90% of available amino groups of whey proteins. Details about the structural characterisation of the hydrophobised WPI have been provided elsewhere (Madadlou, Floury, & Dupont, 2018). The modified product was then used to form a water-in-water (W/W) emulsion of alginate and WPI, which was attributed to the adsorption of protein particles to the liquid-liquid interface. The interfacial tension between the two incompatible biopolymer phases was further modulated by addition of erythritol, a low-calorie sugar alcohol (Madadlou, Saint-Jalmes, Guyomarc'h, Floury, & Dupont, 2019).

Adsorption of macromolecules and particles to the liquid/liquid interface during emulsification forms a viscoelastic layer, which can be assessed by shear rheology components (elasticity and viscosity). Shear rheology characterises the response of the

(particle-laden) interface to a shape deformation caused by an external mechanical perturbation, in a similar way done for bulk rheology (Mendoza et al., 2014). Inter-particle attractive and repulsive forces such as electrostatic and hydrophobic interactions govern the interface rheology. Indeed, interfacial rheology is very sensitive to the structure and composition of a protein layer formed at the interface, as well as to the nature of interactions within the layer (Dickinson & Matsumura, 1991). Therefore, it was presumed that probing interfacial rheology is advantageous for assessing the emulsification behaviour of whey proteins as influenced by hydrophobisation.

Rheological analysis is also helpful to study the gelation properties of whey proteins. Cold-set gelation of whey proteins is of great value in forming particles that can modify viscosity (Zhang et al., 2018), and encapsulate heat-labile cargos (Farjami, Madadlou, & Labbafi, 2016; Hashemi, Madadlou, & Salami, 2017). This property can also be used to form whey protein-stabilised emulsion gels for fortification and technological purposes. For example, such emulsions can be incorporated into cultured milk products like yoghurt to improve texture (Boutin, Giroux, Paquin, & Britten, 2007). The cold-set gelation process takes place by a two-step consecutive procedure. Initially, the proteins are heat-denatured at non-gelling conditions (i.e., at low ionic strength, low protein content and at pH values far from the proteins' isoelectric point, pI), which causes formation of whey protein soluble aggregates. Then the protein dispersion is gelled at ambient temperature by adding salts and/or adjusting pH toward the pI (Ju & Kilara, 1998; Meydani, Vahedifar, Askari, & Madadlou, 2019). The rheology of such gels is governed by the interaction between the aggregating protein particles, which is highly dependent on the aggregate chemistry (Alting, Hamer, De Kruif, & Visschers, 2003). Therefore, the modification of whey proteins via hydrophobisation is expected to alter the cold-set gelation behaviour and the gel rheology of WPI.

The first objective of the present study was to analyse the interfacial rheology of WPI at the air-liquid interface as influenced by heat denaturation and hydrophobisation treatments, as well as, erythritol (E) addition into the hydrophobised WPI. Subsequently, bulk rheological experiments were carried out to assess the acid-induced cold-set gelation process and the gel properties of the hydrophobised WPI (with and without E) and the alginate-supplemented E-added hydrophobised WPI (i.e., W/W emulsion).

2. Materials and methods

2.1. Materials

WPI was received as a gift from Lactalis ingredients (Bourgbarré, France). It contained, according to the information provided by the manufacturer, 90% protein, 5.1% water, 3.0% lactose, and 1.97% ash. Reversed-phase high-performance liquid chromatography (RP-HPLC) analysis indicated that the α-lactalbumin and β-lactoglobulin content of the WPI was 16% and 56% of total protein, respectively. Erythritol was purchased from Vita-World GmbH (Taunusstein, Germany). Alginic acid sodium salt from brown algae was procured from Sigma-Aldrich (SKU W201502, Sigma-Aldrich Chemie S.a.r.l., Saint-Quentin Fallavier, France). Sodium hydroxide and hydrochloric acid were bought from Sigma-Aldrich. Ultrapure, 15 mΩ-resistivity water prepared by reverse osmosis was used throughout the study and all chemicals were analytical grade.

2.2. Protein modification, emulsion preparation and gelation

WPI was hydrophobised following the method described in our previous report (Madadlou et al., 2018). Briefly, WPI powder was hydrated (65 mg mL^{-1}) for 18 h and supplemented with acetic anhydride at a ratio of 0.18 g g^{-1} protein. After 30 min acetylation while the pH was kept over 8.0 through successive additions of 1 M NaOH, the WPI dispersion was heated at 85 °C for 20 min. A non-acetylated but heat-denatured WPI sample was also prepared by sequentially adding 1 M HCl (200 μL), and 1 M NaOH (300 μL) to a native WPI dispersion (9.5 mL, pH 6.7) to set pH to 8.25 ± 0.05, and subsequent heat treatment at 85 °C for 20 min. The sequential addition of the acid and alkali was carried out to mimic the fall and rise of pH during the hydrophobisation process. After heat treatment, the pH value of the hydrophobised and heat-denatured WPI samples was adjusted to 7.50 ± 0.05 using approximately 20 μL of either 1 M HCl or 1 M NaOH.

The alginate-in-WPI W/W emulsions were prepared according to the method described elsewhere (Madadlou et al., 2019) with minor changes. At first, erythritol was added (100 mg mL^{-1}) into the hydrophobised WPI dispersion and stirred, followed by addition of sodium alginate solution (30 mg mL^{-1}) into WPI-erythritol mixture at a volume ratio of 1:9. The mixture was vortexed at a rotating frequency of 40 Hz (Bioblock Top Mix 11118, Fisher Scientific, Waltham, MA, USA) for 90 s to obtain the W/W emulsion.

The hydrophobised (with and without added erythritol) and heat-denatured WPI samples, as well as the alginate-in-WPI mixed (i.e., W/W emulsion) system (pH 7.50 ± 0.1) were gelled at 37 °C by acidification. Glucono-δ-lactone (GDL) was added (5, 10 and 20 mg mL^{-1}) into the samples to gradually hydrolyse into gluconic acid, causing acid gel formation. The samples were stored at 37 °C for 24 h before analyses. The pH value of the samples during gelation was monitored using a digital pH meter (CyberScan Series pH 110, Eutech Instrument, Singapore). The accuracy of the pH measurement was ±0.02 pH unit.

142 *2.3. Interfacial shear measurements*

143

144 A stress-controlled rheometer (Discovery Series Hybrid Rheometer (DHR) HR-2,
145 New Castle, DE, USA) using the double wall ring (DWR) geometry was used to perform the
146 interfacial shear analyses including strain amplitude sweep and creep tests. The WPI sample
147 was poured into a round trough and an annular ring made of a platinum–iridium alloy was
148 positioned at the liquid–air interface. The DWR geometry has been thoroughly described
149 (Vandebril, Franck, Fuller, Moldenaers, & Vermant, 2010) and provides certainty that high
150 values of the Boussinesq number are attained. Therefore, the contribution of the induced sub-
151 phase flow to torque is negligible and the interfacial torque dominates (Jaishankar &
152 McKinley, 2013). Based on time sweep tests at a strain amplitude of 0.1% and an angular
153 frequency of 10 rad s^{-1} and on the literature review (Jaishankar et al., 2011), all steady state
154 experiments were carried out after waiting for 3 h at 20 °C. WPI dispersions (56 mg mL^{-1})
155 were loaded into the trough, the annular ring was positioned at the interface and after the rest
156 period, the experiments were carried out.

157 It is noteworthy that in the current study, the interfacial shear rheology of WPI
158 dispersions was analysed at the same concentration as emulsion preparation was done.
159 Commonly, the interfacial rheology tests are performed at much lower concentrations of
160 amphiphilic compounds to make sure that a monolayer of the compounds is present at the
161 interface. However, as noted earlier (Lexis & Willenbacher, 2014), the structure of the
162 interfacial layers of proteins depends largely on concentration; therefore, a correlation
163 between properties such as foaming and emulsification, and interfacial rheology is achieved
164 only when the interfacial layers at both conditions (i.e., emulsion formation and interfacial
165 rheology test) are comparable. Nonetheless, as the thickness of the interfacial layer may not
166 be negligible anymore, the measured moduli are treated as apparent values. Similar

concentrations have already been used for the interfacial rheological analysis of bovine serum albumin (Jaishankar & McKinley, 2013; Jaishankar et al., 2011; Sharma, Jaishankar, Wang, & McKinley, 2011).

After amplitude sweep tests, creep tests were performed on WPI interfacial layers over short durations. In stress-controlled rheometry, for sufficiently viscoelastic fluids, even if they are simple Newtonian fluids, a ringing event (i.e., damped oscillations) is observed at the start of a creep test (Ewoldt & McKinley, 2007). The coupling of fluid elasticity and instrument inertia causes periodic oscillations which decay exponentially due to viscous dissipation (Jaishankar & McKinley, 2013). The creep ringing logarithmic decrement, Δ and ringing frequency, ω_* (Nagarkar et al., 2009) of WPI interfacial layers were calculated (where applicable) using the following equations:

$$\Delta = 2ln\left[\frac{(J_1 - J_2)}{(J_3 - J_2)}\right] \quad \text{[Eq. 1]}$$

$$\omega_* = \frac{1}{(t_3 - t_1)} \quad \text{[Eq. 2]}$$

where J_1, J_2, and J_3 are the compliance values of the 1st peak, 1st valley and 2nd peak of the creep ringing data, respectively (Nagarkar et al., 2009) and $t_3$and $t_1$are the times of the 2nd peak and 1st peak, respectively.

2.4. Particle size and ζ-potential of WPI dispersions during gelation

The hydrodynamic diameter and ζ-potential of protein particles during gelation were approximated by dynamic light scattering (DLS) following the methods of Ju and Kilara (1998) and de Jong, Klok, and van de Velde (2009a) for acid-induced gelation of whey proteins. A Zetasizer Nano ZS (Malvern Instruments Ltd., Worcestershire, UK) was used for this purpose. Protein samples (at 37 °C) were supplemented with GDL (20 mg mL^{-1} for hydrophobised WPI and 5 mg mL^{-1} for heat-treated WPI), and stored at 37 °C (de Jong, Klok,

& van de Velde, 2009b) for different durations, i.e., 130 min for the hydrophobised WPI samples and 35 min for the heat-denatured WPI. At various time intervals, the samples were diluted 100 fold with deionised water and subjected to DLS analysis. Dilution did not have a remarkable influence (less than 0.2 unit) on the pH value of the samples. The refractive index of dispersant (water) was 1.33, and the dispersant viscosity was set to 0.69 mPa s. A laser-backscattering angle of 173° and a wavelength of 633 nm were applied in size measurements.

2.5. Rheological analyses of WPI and alginate-WPI gel samples

The gelation time (Ti_g) and rheological properties of WPI and emulsion samples were determined using an Anton Paar Physica MCR 301 rheometer (Anton Paar GmbH, Graz, Austria) equipped with a cone-plate geometry (diameter 49.96 mm and cone angle 1.99°). Samples supplemented with GDL (20 mg mL^{-1} for the hydrophobised WPI and the emulsion and 5, 10, and 20 mg mL^{-1} for the heat-denatured WPI) were poured onto the plate, followed by introducing the cone. Temperature was kept at 37 °C. Low-density paraffin was added around the samples to prevent evaporation. Changes in storage modulus (G′), loss modulus (G″), and damping factor (tan δ) during gelation of the samples were measured at an angular frequency of 1 rad s^{-1} and 0.1% strain. Gelation time (Ti_g) was arbitrarily defined as G′ = 1 Pa (Andoyo, Guyomarc'h, & Famelart, 2016). Gels were oscillated in situ for 24 h to obtain a fully developed network. Then, a frequency sweep test was performed to determine the effect of time scale of deformation on the rheological properties when the samples were formed (Lee & Lucey, 2003). Frequency was increased from 0.0628 to 628 rad s^{-1} at 0.1% strain and 37 °C.

2.6. Confocal laser scanning microscopy

Confocal laser scanning microscopy (CLSM) observation of gel microstructure was performed using the ZEISS LSM 880 inverted confocal microscope (Carl Zeiss AG, Oberkochen, Germany) set at magnification 63× (Plan Apochromat objective, oil immersion, NA 1.4) using the Airyscan detection unit. The dispersion of WPI and emulsion containing GDL were mixed with a 1% (w/v) solution of Fast Green at a ratio of 9:1. Each sample (1 mL) was injected into the chamber of a gel cassette® system (Brocklehurst, Mackie, Steer, & Wilson, 1998) and vertically incubated at 37 °C for 24 h. After gelification, Airyscan images were acquired using a He/Ne laser with a wavelength of 633 nm, using with a main beam splitter MBS488/561/633 and no additional emission filter. The zoom was set at 4 for gel imaging and 1.8 for W/W emulsion sample. For further image analysis of W/W emulsion, ten micrographs of 1336×1336 pixels (1 µm = 18.17 pixels) were taken on different regions in a constant z-position. Zen Black 2.1 (Version 13.0.0.0) software was used to process the acquired datasets using the 2D mode at default settings of the Airyscan processing function, including a Wiener filter deconvolution.

Airyscan confocal micrographs of the W/W emulsions were converted to binary images using the "Default" thresholding algorithm of Fiji-win64 software. The segmentation procedure was validated by visual comparison of the resulted binary image with its original image. The particle areas were measured using the Analyze Particles measurements tool (in µm²). Corresponding diameters were calculated, based on the hypothesis that all particles were spherical.

2.7. Statistical analysis

241 Samples were prepared in triplicate and the experiments were done at least two times.
242 The results were analysed by one-way ANOVA with SPSS software version 16 (IBM
243 software, New York, NY, USA) using Duncan's test at a significance level of P <0.05.
244
245 **3. Results and discussion**
246
247 *3.1. Interfacial rheology*
248
249 *3.1.1. Amplitude sweep*
250 The dynamic moduli of air-WPI interfaces were first measured over time at a fixed
251 strain amplitude and oscillation frequency. The interfacial shear storage (G_s') and loss (G_s'')
252 moduli reached equilibrium 2–3 h after sample loading, which indicates that the structure of
253 interface reached steady state (Jaishankar & McKinley, 2013). Then, small amplitude
254 oscillatory strain sweeps were carried out to find out the onset of non-linearity of the samples
255 viscoelastic response. Typical curves of the results of strain sweep tests are illustrated in Fig.
256 1. In agreement with the literature on native β-lactoglobulin (Ridout, Mackie, & Wilde, 2004),
257 the G_s' of the air-liquid interfacial layer of native WPI had a value of about 13 mN m^{-1} (Table
258 1). Heat denaturation and hydrophobisation decreased the G_s' value of the air-liquid interfacial
259 layer of WPI. Native β-lactoglobulin, as the major whey protein, when adsorbed at interface
260 polymerises over time, concomitant with lack of any appreciable exchange between adsorbed
261 polymers and non-adsorbed monomers. The polymerisation takes place by the gradual
262 exposure of the free –SH groups embedded in the interior of the molecule, triggering
263 progressive formation of disulphide crosslinks. It develops a remarkable extent of β-
264 lactoglobulin oligomers at interface 2 h after interfacial adsorption (Dickinson & Matsumura,
265 1991).

In contrast to native proteins, extensive conformational changes and disulphide bond formation take place before interfacial adsorption in heat-processed proteins (Meydani et al., 2019), i.e., the heat-denatured and hydrophobised WPI samples. This reduces the extent of permanent crosslinks formation after interfacial adsorption. Furthermore, the greater absolute values of negatively signed ζ-potentials of heat-denatured and hydrophobised WPIs in comparison with native WPI at comparable pH values (Madadlou et al., 2018) suggest a stronger electrostatic repulsion between protein particles at the interfacial layer, reducing the stiffness and hence the G_s' of the layer. Likewise, a smaller extent of crosslinking between protein molecules was argued to explain the lower interfacial viscosity of β-lactoglobulin at the air-water interface when compared with oil-water interface (Roth, Murray, & Dickinson, 2000).

The point at which G_s' deviated by more than 10% from a constant value was considered as the onset of non-linearity (TA Instruments, New Castle, DE, USA: http://www.tainstruments.com/pdf/literature/RS23.pdf), which took place at a strain amplitude of 1.8%, 1.6%, and 1.2% for the air-liquid interfacial layers of native, heat-denatured and hydrophobised WPI samples, respectively. For these three samples, a shorter linear region coincided a lower G_s' value (Table 1).

Although erythritol addition slightly decreased the G_s' and G_s'' of the hydrophobised WPI interfacial layer, the reduction was not statistically significant (Fig. 1; Table 1). Likewise, the phase-shift angle, δ of the layer was not influenced by erythritol addition (Table 1). Furthermore, the δ values of the air-liquid interfacial layers of the hydrophobised WPI samples (either E-free or E-added) were not different from that of the heat-denatured sample. In contrast, native WPI had a remarkably smaller δ in the linear region. Within the linear region, G_s' was larger than G_s'' for all samples, indicating that the interfacial layers were predominately elastic (Langevin, 2000; Sharma et al., 2011).

All interfacial layers underwent a yielding process at high strain amplitudes. The process is shown by a steep collapse in the magnitude of G_s' and the domination of G_s'' beyond a certain amplitude (Jaishankar et al., 2011). The values of oscillation flow stress (τ_f) and flow strain (γ_f) of the WPI interfacial layers were affected by heat denaturation and hydrophobisation. The crossovers of G_s' and G_s'', which indicate the flow points of the interfacial layers, are specified by the circles in Fig. 1, and the corresponding τ_f and γ_f values are reported in Table 1. In accordance with the influence on G_s', heat-denaturation and hydrophobisation decreased the values of τ_f and γ_f of the interfacial layer, and erythritol addition into the hydrophobised WPI did not influence the flow-point criteria (i.e., τ_f and γ_f) of the air-liquid interfacial layer. Again, hydrophobisation caused a greater reduction of the flow-point criteria than heat denaturation.

3.1.2. Creep ringing

The creep compliance of the interfacial layers as a function of time at different magnitudes of interfacial stress, τ_s over a few seconds is illustrated in Fig. 1. A typical creep ringing behaviour, i.e., damping free oscillation, is observed for the interfacial film of native WPI. In the linear regime, strain is a linear function of stress; hence, the compliance curves should overlap for an ideal linear viscoelastic material. This happened at times shorter than 2 s for the interfacial layer of native WPI and indicates that the elastic component of the sample controls the first instant response, causing comparable ringing behaviours irrespective of the value of applied τ_s (Goudoulas & Germann, 2016). Likewise, the creep compliance curves of polyacrylamide solutions (Goudoulas & Germann, 2016) and bovine serum albumin interfacial films (Jaishankar et al., 2011) deviated at periods longer than 2 s and 5 s, respectively, indicating the onset of non-linear behaviour and the domination of viscous component.

316 Creep ringing was weakly observed for the air-liquid interfacial film of the heat-
317 denatured WPI. In addition, the compliance curves of this sample (heat-denatured WPI)
318 commenced to deviate only after 0.8 s. The interfacial films of the hydrophobised WPI and
319 the E-added hydrophobised WPI did not show any creep ringing property. Indeed, to observe
320 creep ringing, the sample must have sufficient elasticity, so that $G_J > G_{criticial}$, where G_J is the
321 modulus of spring in the Jeffreys model (Ewoldt & McKinley, 2007). Therefore, the absence
322 of the ringing property in the air-water interfacial layers of the hydrophobised WPIs (with and
323 without added erythritol) agrees with the results of the strain amplitude oscillatory test.
324 Δ and ω_* values of the interfacial layer of native WPI-air were 0.125 ± 0.010 and 1.17 ± 0.06
325 Hz, respectively. The short time creep response is quadratic in time and according to Struick's
326 formula, the interfacial elastic modulus is proportional to the square of ω_* (Jaishankar et al.,
327 2011):

328 $$G_s' \approx \alpha_s \omega_*^2 \left[1 + \left(\frac{\Delta}{2\pi}\right)^2\right] \qquad \text{[Eq. 3]}$$

329 The parameter $\alpha_s = \frac{I}{b}$ is an instrumentation parameter and remains unchanged for the
330 samples because the total moment of inertia (I) of the system and the factor b which is
331 determined by the geometry are identical. The ratio of the square values of ω_* of native WPI-
332 air layer was 2.25, which is very close to the ratio of the samples G_s' values in the linear
333 region, i.e., 2.35. This indicates that the linear elastic modulus can be directly determined
334 using the data from the creep ringing test.
335
336 *3.2. Buffering capacity and particle size of WPI during acid gelation*
337
338 Interfacial rheology analyses indicated that hydrophobisation decreased the dynamic
339 moduli of air-liquid interfacial layers of WPI. Next, we assessed the influence of

hydrophobisation on the acid-induced cold-set gelation properties of WPI using bulk rheology. The WPI samples and the W/W emulsion produced were gelled with GDL. The pH value of the heat-denatured WPI supplemented with GDL at a level of 20 mg mL^{-1} decreased to ≈3.8, after acidification for 130 min, whereas its value for hydrophobised WPI supplemented with a comparable GDL concentration (20 mg mL^{-1}) decreased only to 5.07 after an identical period of time (results not shown). On the other hand, the acidification profiles (pH versus time) of the heat-denatured and hydrophobised WPI samples supplemented with GDL at the respective concentration of 5 mg mL^{-1} and 20 mg mL^{-1} were very close. Therefore, the buffering capacity (i.e., resistance to pH changes) of whey proteins increased due to hydrophobisation.

The carboxylic acid group of amino acids has a pK_a value of approximately 2.3, which is significantly lower than the pK_a value (4.8) of acetic acid due to negative inductive (electron withdrawing) effect on the carboxylic acid group by the $-NH_3^+$ group. Accordingly, the carboxyl acid group of α-amino acids is about 300 times stronger an acid than acetic acid. In proteins and peptides, the pK_a of terminal α-carboxyl groups is 3.1–3.8 (intermediate between the carboxylic acid groups of acetic acid and glycine) because of the lower negative inductive effect of proximal peptide bond rather than the $-NH_3^+$ group in an α-amino acid. It is noteworthy that the β and γ carboxylic acid groups of aspartic (pK_a = 3.9) and glutamic (pK_a = 4.3) acids are somewhat insulated from these electronic effects by intervening saturated carbons (Barrett & Elmore, 1998). Hydrophobisation, which occurred through the acetylation of a great majority (>90%) of free amino groups of whey proteins (Madadlou et al., 2018), decreased the inductive effect and increased the pK_a values of terminal carboxylic acid groups. A large amount of acid or base is needed to change pH near the pK_a, so that buffer solutions are stronger at pH levels near their pK_a values (Shimadzu Corporation, 2015). The hydrophobised WPI that had a higher pK_a value was a stronger buffer and required a 4-fold

higher amount of GDL to undergo an acidification profile comparable with that of the heat-denatured WPI.

During formation of acid-induced protein gels, reduction of pH towards the pI decreases the net negative charge on protein particles. Then, the particles begin to crosslink, forming clusters of different but finite size. At a certain threshold of interconnection, the final gel network is formed (Madadlou, Emam-Djomeh, Mousavi, Mohamadifar, & Ehsani, 2010). The particle size of WPI dispersions was measured during acidification immediately after GDL addition. The hydrophobised protein particles had a mean hydrodynamic diameter of approximately 82 nm, 3 min after GDL addition. Fig. 2A indicates that during the acidification, the particle size of hydrophobised WPI initially decreased, followed by a progressive increase over the rest of acidification. Plotting the mean hydrodynamic diameter of protein particles versus mean pH during acidification until gel formation time (Fig. 2B) indicated that the size of hydrophobised protein particles decreased with decreasing pH to approximately 5.5 (identified by an arrow in Fig. 2B). This pH value corresponded to 30 min after GDL addition. Likewise, the particle diameter of heat-denatured WPI showed a small reduction in the beginning of acidification, followed by a remarkable increase (Fig. 2A). As soon as GDL was added, the pH value of WPI dispersions sharply decreased (results not shown), and then reached a plateau after gel formation over long durations. The initial reduction and the subsequent increase of protein particle size during acid gelation, which were observed for both heat-denatured and hydrophobised WPI dispersions are attributed respectively to protein particles shrinkage due to the decrease of intra-particle electrostatic repulsion and succeeding aggregation of the particles.

Erythritol addition did not influence the initial particle size of hydrophobised WPI dispersion, which suggests that erythritol did not interact electrostatically with WPI particles (Madadlou et al., 2019). It did not also affect the aggregate size as a function of pH reduction

(Fig. 2B). However, erythritol addition postponed the onset of aggregation of protein particles to a lower pH value (approximately 5.4) and caused formation of comparatively smaller aggregates just before the gelation point (Fig. 2A).

3.4. Gelation time

Different WPI samples supplemented with GDL (20 mg mL^{-1} for the hydrophobised WPI samples, and 5, 10, and 20 mg mL^{-1} for the heat-denatured WPI) were gelled at 37 °C on a rheometer and the corresponding gelation times are illustrated in Fig. 3A. The heat-denatured WPI gelled approximately 5, 13, and 42 min after adding GDL at respective concentrations of 20, 10, and 5 mg mL^{-1}. The G' values of the heat-denatured WPI gels prepared using GDL at 20 and 10 mg mL^{-1} levels decreased after a peak value (Fig. 3B). The reduction of G' was substantial for the heat-denatured WPI supplemented with 20 mg mL^{-1} GDL, and is attributed to gel disintegration due to over-acidification, which reduced pH to values well below the proteins pI.

Gelation time (t_g) of whey proteins was influenced by hydrophobisation, as well as by erythritol and alginate addition (Fig. 3A). Hydrophobised WPI required about 125 min to gel (pH 5.07 $\pm$ 0.01) after adding GDL at 20 mg mL^{-1}. Erythritol addition, which did not alter the pH value of the hydrophobised WPI, postponed the t_g (Fig. 3A). The E-added hydrophobised WPI gelled approximately 134 min (pH 5.06 $\pm$0.02) after GDL supplementation (20 mg mL^{-1}), which is 9 min longer compared with the counterpart without erythritol. On the contrary, alginate addition into the E-added hydrophobised WPI resulted in a shorter t_g (94 $\pm$ 2 min) in comparison with both E-added and E-free hydrophobised WPIs.

3.5. Dynamic rheology of the WPI gels

The gels developed in situ on the rheometer were subjected to frequency sweep test to gain an insight into their time-dependent behaviour. This rheological analysis is useful to gather information on the internal structure of samples (polymer solutions, gels, emulsions, etc.) and the stability of dispersions during storage. The results of the frequency sweep test are illustrated in Fig. 4. The values of G' and G'' of all samples increased with increasing frequency and G' was greater than G'' at any frequency for all samples, which suggests significant protein-protein interactions at the gels (Zhang et al., 2018) and domination of the elastic component to the viscous one (Madadlou, Khosroshahi, & Mousavi, 2005). However, the difference between the G' and G'' of all gels was smaller than 1 log cycle, indicating that the gels were rather weak (Kamal, Foukani, & Karoui, 2017).

In a manner similar to that of the interfacial rheology results, the hydrophobised WPI gel had lower G' values than the heat-denatured WPI gel throughout the whole frequency range. Moreover, erythritol addition decreased the maximum G' value of the hydrophobised WPI gel in the frequency sweep analysis from approximately 5 kPa to 4 kPa. The G'' of the WPI gel decreased at a comparable extent (≈1.27 fold) due to erythritol addition (Fig. 4). Both E-free and E-added hydrophobised gels had a final (i.e., after 24 h) pH value of 4.75 ± 0.1. Erythritol might interrupt gel network development (Cai, Feng, Regenstein, Lv, & Li, 2017; Torres, Raymundo, & Sousa, 2013). We hypothesise that erythritol increased the hydration of protein particles, reducing the formation of non-covalent bonds (He, Azuma, Hagiwara, & Kanno, 2006) between the particles, impairing gel development. This may explain why the E-added hydrophobised WPI had relatively smaller aggregates than E-free sample just before the gelation point. Although erythritol did not interact with whey proteins (Madadlou et al., 2019), it could increase protein hydration because of excluded volume effect, a phenomenon that weakly depends on the native or denatured state of proteins (Ebel, Eisenberg, &

440 Ghirlando, 2000). Addition of carbohydrates such as sugar alcohols to native protein solutions
441 is known to delay the heat-induced aggregation and gel formation (Wijayanti, Bansal, &
442 Deeth, 2014).

443 In accordance with the influence on gelation time, alginate addition increased the G'
444 and G'' values of the E-added hydrophobised WPI gel. One may assume that alginate gelation
445 along with whey proteins accelerated the gelation and increased gel firmness. Alginate can gel
446 without the aid of calcium (and other multivalent cations) when pH is gradually lowered (for
447 example by GDL) because the fraction of unionised carboxyl groups on the uronic acid
448 residues increases and water is squeezed out (Yotsuyanagi, Yoshioka, Segi, & Ikeda, 1991).
449 Gradual pH reduction is requisite as an abrupt acidification leads to precipitation of alginic
450 acid rather than gel formation. It has been estimated that a minimum alginate concentration of
451 3.5 mg mL^{-1} is needed to obtain a GDL-induced gel (Draget, Skjåk Bræk, & Smidsrød, 1994),
452 which is remarkably lower than the alginate concentration employed in the current study (30
453 mg mL^{-1}), although alginate would partition between the protein-rich and alginate-rich phases
454 of the emulsion (Madadlou et al., 2019).

455 To assess alginate gelation, we added different concentrations of GDL to the alginate
456 solution (30 mg mL^{-1}) and found that a GDL concentration of 1.1 mg mL^{-1} decreased pH after
457 about 90 min (similar to the emulsion t_g) to 5.15 ± 0.04, which is comparable with the
458 emulsion pH at gelation point. Nevertheless, the alginate solution did not gel. The alginate-
459 added WPI gel had a final (after 24 h) pH of approximately 4.75, similar to that of heat-
460 denatured and hydrophobised WPI gels, associated with the protein buffering capacity
461 (Léonard, Husson, Langella, Châtel, & Saurel, 2016). Also, de Jong et al. (2009a) observed a
462 constant pH, independent of polysaccharide type and amount for the acid-induced gels of
463 WPI/polysaccharide mixtures. It was presumed that the continuous and disperse phases of the
464 W/W emulsion had equal pH values (Singh, Medronho, Miguel, & Esquena, 2018). Adding

higher concentrations of GDL, namely 1.4 and 1.7 mg mL^{-1}, decreased pH (after 90 min) to approximately 4.85 and 4.75, respectively; however, gelation did not happen. Indeed, acid gelation of alginate happens at pH values below the pK_a of the uronic acid residues which is approximately 3.7 (Bu, Kjøniksen, & Nyström, 2005).

Although the WPI powder used in the current study contained a small amount of minerals, which could cause alginate hardening/gelation when pH was reduced, the shorter t_g and higher dynamic moduli of alginate-added gel compared with the alginate-free WPI systems is mainly attributed to the microstructural organisation of the composite gel. Likewise, a higher G' of an alginate/caseinate aqueous two-phase system gel than individual gels of either alginate or caseinate was ascribed to the development of a more organised and interconnected structure in the mixed gel (Léonard et al., 2016). Hence, the microstructural features of the samples were assessed to explain the difference between the dynamic moduli of the alginate-added gel and the alginate-free WPI gels.

3.6. Microstructure of the WPI gels

The microstructures of well developed (i.e., stored for 24 h) gel samples were imaged by CLSM and the typical images are depicted in Fig. 5. The polysaccharide-free WPI gels had homogenous microstructures, composed of a protein-rich phase (green) and a serum phase. The latter is observed as black micro-channels interconnected throughout the gel matrix. Microscopic images (Fig. 5) showed that alginate was dispersed as droplets in a continuous matrix of proteins. Micro-phase separation of protein-polysaccharide pairs is usual and known to increase the firmness of the subsequently formed protein gels (Zand-Rajabi & Madadlou, 2016). Micro-phase separation concentrates the incompatible polymers in separated domains, causing higher effective concentrations than nominal (Beaulieu, Turgeon, & Doublier, 2001).

The diameter of approximately 1700 droplets were measured and the result is illustrated in Fig. 5. The emulsion gel droplet size was highly inhomogeneous and droplets as large as 20 μm were present. It is also observed in Fig. 5D that some adjacent alginate droplets were in contact and partially coalesced. Modification of the gelation method might be helpful to confine the droplet disproportionation kinetics.

5. Conclusions

Hydrophobisation of whey proteins through acetylation decreased the liquid-air interfacial viscoelasticity of WPI. Air is a very hydrophobic medium. Hence, concurrent reduction of the interfacial elasticity (observed in the current study) and interfacial tension (observed in a previous study; Madadlou et al., 2019) of hydrophobised WPI at the liquid-air interface indicates that more hydrophobic protein particles which accumulated at the interface were less elastic. An opposite process took place in the alginate-protein emulsions, i.e. more elastic but less hydrophobic protein particles stabilised the all-aqueous interfaces. This conclusion relies on the assumption that at least two populations of particles with different hydrophobicities were present at the protein phase. It is noteworthy that macroscopic phase separation of non-gelled W/W emulsions is conventionally slowed down by accumulation of third component particles at the water-water interface. However, as communicated in an earlier report (Madadlou et al., 2019), stable W/W emulsions can be made using a pair consisting of only hydrophobised protein and a co-charged polysaccharide without a third component. The fabrication of the two-component stable W/W emulsions is thrilling. Should the above-mentioned conclusion be correct, one may design a wide range of two-component (protein and polysaccharide only) stable and fluid (not gelled) W/W emulsions by masterful manipulation of the shape, size, and surface hydrophobicity of protein particles. Acidification

of the emulsion produced soft gels which might be used for encapsulation of drugs, nutraceuticals and enzymes as two-phase oil-free systems. In addition, the emulsion could be utilised to perform reactions at the interface of two discrete, but interfacially touching, aqueous phases. Addition of erythritol to the hydrophobised WPI dispersion, which facilitated emulsification, resulted in an inferior interfacial and gel viscoelasticity. Therefore, it is possible to tune the interfacial and gel viscoelasticity of hydrophobised WPI and the W/W emulsions using a non-caloric sweetener.

Acknowledgements

The authors are thankful to the support of the EU in the framework of the Marie-Curie FP7 COFUND People Programme, through the award of an AgreenSkills+ fellowship (grant agreement n°609398). The ZEISS LSM880 confocal microscope equipped with the Fast Airyscan detector was funded by the European Union (FEDER), the French Ministry of Education, Research and Innovation, the Regional Council of Brittany and INRA.

References

Alting, A. C., Hamer, R. J., De Kruif, C. G., & Visschers, R. W. (2003). Cold-set globular protein gels: Interactions, structure and rheology as a function of protein concentration. *Journal of Agricultural and Food Chemistry*, *51*, 3150–3156.

Andoyo, R., Guyomarc'h, F., & Famelart, M. H. (2016). Acid gelation of whey protein microbeads of different sizes. *Dairy Science and Technology*, *96*, 213–225.

Barrett, G. C., & Elmore, D. T. (1998). *Amino acids and peptides*. Cambridge, UK: Cambridge University Press.

Beaulieu, M., Turgeon, S. L., & Doublier, J. L. (2001). Rheology, texture and microstructure of whey proteins/low methoxyl pectins mixed gels with added calcium. *International Dairy Journal*, *11*, 961–967.

Boutin, C., Giroux, H. J., Paquin, P., & Britten, M. (2007). Characterisation and acid-induced gelation of butter oil emulsions produced from heated whey protein dispersions. *International Dairy Journal*, *17*, 696–703.

Brocklehurst, T. F., Mackie, A. R., Steer, D. C., & Wilson, D. R. (1998). Detection of microbial growth. *US patent US5739003A*.

Bu, H., Kjøniksen, A. L., & Nyström, B. (2005). Effects of pH on dynamics and rheology during association and gelation via the Ugi reaction of aqueous alginate. *European Polymer Journal*, *41*, 1708–1717.

Cai, L., Feng, J., Regenstein, J., Lv, Y., & Li, J. (2017). Confectionery gels: Effects of low calorie sweeteners on the rheological properties and microstructure of fish gelatin. *Food Hydrocolloids*, *67*, 157–165.

de Jong, S., Klok, H. J., & van de Velde, F. (2009a). The mechanism behind microstructure formation in mixed whey protein-polysaccharide cold-set gels. *Food Hydrocolloids*, *23*, 755–764.

de Jong, S., Klok, H. J., & van de Velde, F. (2009b). The mechanism behind microstructure formation in mixed whey protein–polysaccharide cold-set gels. *Food Hydrocolloids*, *23*, 755–764.

Dickinson, E., & Matsumura, Y. (1991). Time-dependent polymerization of β-lactoglobulin through disulphide bonds at the oil-water interface in emulsions. *International Journal of Biological Macromolecules*, *13*, 26–30.

Draget, K. I., Skjåk Bræk, G., & Smidsrød, O. (1994). Alginic acid gels: the effect of alginate chemical composition and molecular weight. *Carbohydrate Polymers*, *25*, 31–38.

565 Ebel, C., Eisenberg, H., & Ghirlando, R. (2000). Probing protein-sugar interactions.
566 *Biophysical Journal*, *78*, 385–393.
567 Ewoldt, R. H., & McKinley, G. H. (2007). Creep ringing in rheometry or how to deal with
568 oft-discarded data in step stress tests! *Rheology Bulletin*, *76*, 4–6.
569 Farjami, T., Madadlou, A., & Labbafi, M. (2016). Modulating the textural characteristics of
570 whey protein nanofibril gels with different concentrations of calcium chloride. *Journal*
571 *of Dairy Research*, *83*, 109–114.
572 Foegeding, E. A., Davis, J. P., Doucet, D., & McGuffey, M. K. (2002). Advances in
573 modifying and understanding whey protein functionality. *Trends in Food Science &*
574 *Technology*, *13*, 151–159.
575 Goudoulas, T. B., & Germann, N. (2016). Viscoelastic properties of polyacrylamide solutions
576 from creep ringing data. *Journal of Rheology*, *60*, 491–502.
577 Hashemi, B., Madadlou, A., & Salami, M. (2017). Functional and in vitro gastric digestibility
578 of the whey protein hydrogel loaded with nanostructured lipid carriers and gelled via
579 citric acid-mediated crosslinking. *Food Chemistry*, *237*, 23–29.
580 He, J.-S., Azuma, N., Hagiwara, T., & Kanno, C. (2006). Effects of sugars on the cross-
581 linking formation and phase separation of high-pressure induced gel of whey protein
582 from bovine milk. *Bioscience, Biotechnology, and Biochemistry*, *70*, 615–625.
583 Jaishankar, A., & McKinley, G. H. (2013). Power-law rheology in the bulk and at the
584 interface: quasi-properties and fractional constitutive equations. *Proceedings of the*
585 *Royal Society A: Mathematical, Physical and Engineering Sciences*, *469*, Article
586 2012.0284.
587 Jaishankar, A., Sharma, V., & McKinley, G. H. (2011). Interfacial viscoelasticity, yielding
588 and creep ringing of globular protein-surfactant mixtures. *Soft Matter*, *7*, 7623–7634.

589 Ju, Z. Y., & Kilara, A. (1998). Gelation of pH-aggregated whey protein isolate solution
590 induced by heat, protease, calcium salt, and acidulant. *Journal of Agricultural and*
591 *Food Chemistry*, *46*, 1830–1835.
592 Kamal, M., Foukani, M., & Karoui, R. (2017). Effects of heating and calcium and phosphate
593 mineral supplementation on the physical properties of rennet-induced coagulation of
594 camel and cow milk gels. *Journal of Dairy Research*, *84*, 220–228.
595 Langevin, D. (2000). Influence of interfacial rheology on foam and emulsion properties.
596 *Advances in Colloid and Interface Science*, *88*, 209–222.
597 Lee, W. J., & Lucey, J. A. (2003). Rheological properties, whey separation, and
598 microstructure in set-style yogurt: Effects of heating temperature and incubation
599 temperature. *Journal of Texture Studies*, *34*, 515–536.
600 Léonard, L., Husson, F., Langella, P., Châtel, J.-M., & Saurel, R. (2016). Aqueous two-phase
601 system cold-set gelation using natural and recombinant probiotic lactic acid bacteria as
602 a gelling agent. *Colloids and Surfaces B: Biointerfaces*, *141*, 338–344.
603 Lexis, M., & Willenbacher, N. (2014). Relating foam and interfacial rheological properties of
604 β-lactoglobulin solutions. *Soft Matter*, *10*, 9626–9636.
605 Liu, X., Powers, J. R., Swanson, B. G., Hill, H. H., & Clark, S. (2005). Modification of whey
606 protein concentrate hydrophobicity by high hydrostatic pressure. *Innovative Food*
607 *Science & Emerging Technologies*, *6*, 310–317.
608 Madadlou, A., Emam-Djomeh, Z., Mousavi, M. E., Mohamadifar, M., & Ehsani, M. (2010).
609 Acid-induced gelation behavior of sonicated casein solutions. *Ultrasonics*
610 *Sonochemistry*, *17*, 153–158.
611 Madadlou, A., Floury, J., & Dupont, D. (2018). Structural assessment and catalytic oxidation
612 activity of hydrophobized whey proteins. *Journal of Agricultural and Food Chemistry*,
613 *66*, 12025–12033.

614 Madadlou, A., Khosroshahi, A., & Mousavi, M. E. (2005). Rheology, microstructure, and
615 functionality of low-fat Iranian white cheese made with different concentrations of
616 rennet. *Journal of Dairy Science*, *88*, 3052–3062.
617 Madadlou, A., Saint-Jalmes, A., Guyomarc'h, F., Floury, J., & Dupont, D. (2019).
618 Development of an aqueous two-phase emulsion using hydrophobized whey proteins
619 and erythritol. *Food Hydrocolloids*, *93*, 351–360.
620 Mendoza, A. J., Guzmán, E., Martínez-Pedrero, F., Ritacco, H., Rubio, R. G., Ortega, F., et al.
621 (2014). Particle laden fluid interfaces: Dynamics and interfacial rheology. *Advances in*
622 *Colloid and Interface Science*, *206*, 303–319.
623 Meydani, B., Vahedifar, A., Askari, G., & Madadlou, A. (2019). Influence of the Maillard
624 reaction on the properties of cold-set whey protein and maltodextrin binary gels.
625 *International Dairy Journal*, *90*, 79–87.
626 Nagarkar, S., Patil, A., Lele, A., Bhat, S., Bellare, J., & Mashelkar, R. A. (2009). Some
627 mechanistic insights into the gelation of regenerated silk fibroin sol. *Industrial and*
628 *Engineering Chemistry Research*, *48*, 8014–8023.
629 Ridout, M. J., Mackie, A. R., & Wilde, P. J. (2004). Rheology of mixed β-casein/β-
630 lactoglobulin films at the air-water interface. *Journal of Agricultural and Food*
631 *Chemistry*, *52*, 3930–3937.
632 Roth, S., Murray, B. S., & Dickinson, E. (2000). Interfacial shear rheology of aged and heat-
633 treated β-lactoglobulin films: Displacement by nonionic surfactant. *Journal of*
634 *Agricultural and Food Chemistry*, *48*, 1491–1497.
635 Sharma, V., Jaishankar, A., Wang, Y. C., & McKinley, G. H. (2011). Rheology of globular
636 proteins: Apparent yield stress, high shear rate viscosity and interfacial viscoelasticity
637 of bovine serum albumin solutions. *Soft Matter*, *7*, 5150–5160.

638 Shimadzu Corporation. (2015). pKa and Dissociation Equilibrium: SHIMADZU. Retrieved
639 from http://www.shimadzu.com/an/hplc/support/lib/lctalk/29/29intro.html
640 Singh, P., Medronho, B., Miguel, M. G., & Esquena, J. (2018). On the encapsulation and
641 viability of probiotic bacteria in edible carboxymethyl cellulose-gelatin water-in-water
642 emulsions. *Food Hydrocolloids*, *75*, 41–50.
643 Torres, M. D., Raymundo, A., & Sousa, I. (2013). Effect of sucrose, stevia and xylitol on
644 rheological properties of gels from blends of chestnut and rice flours. *Carbohydrate*
645 *Polymers*, *98*, 249–256.
646 Vandebril, S., Franck, A., Fuller, G. G., Moldenaers, P., & Vermant, J. (2010). A double wall-
647 ring geometry for interfacial shear rheometry. *Rheologica Acta*, *49*, 131–144.
648 Wijayanti, H. B., Bansal, N., & Deeth, H. C. (2014). Stability of whey proteins during thermal
649 processing: A review. *Comprehensive Reviews in Food Science and Food Safety*, *13*,
650 1235–1251.
651 Yotsuyanagi, T., Yoshioka, I., Segi, N., & Ikeda, K. (1991). Acid-induced and calcium-
652 induced gelation of alginic acid: bead formation and pH-dependent swelling.
653 *Chemical & Pharmaceutical Bulletin*, *39*, 1072–1074.
654 Zand-Rajabi, H., & Madadlou, A. (2016). Caffeine-loaded whey protein hydrogels reinforced
655 with gellan and enriched with calcium chloride. *International Dairy Journal*, *56*, 38–
656 44.
657 Zhang, Z., Arrighi, V., Campbell, L., Lonchamp, J., & Euston, S. R. (2018). Properties of
658 partially denatured whey protein products: Viscoelastic properties. *Food*
659 *Hydrocolloids*, *80*, 298–308.
660 Zhao, Y., Ma, C.-Y., Yuen, S.-N., & Phillips, D. L. (2004). Study of succinylated food
661 proteins by Raman Spectroscopy. *Journal of Agricultural and Food Chemistry*, *52*,
662 1815–1823.

Figure legends

Fig. 1. Interfacial strain sweep (A, C, E, G) and creep (B, D, F, H) tests of whey protein isolate (WPI) samples: A and B, native WPI; C and D, heat denatured WPI; E and F, hydrophobised WPI; G and H, erythritol-added hydrophobised WPI. The interfacial shear storage (G_s') and loss (G_s'') moduli are shown by ● and ■, respectively. The dashed line (strain sweep results) indicates the onset of non-linear viscoelasticity and the dashed circle specifies the crossover of the dynamic moduli. The creep tests were performed at three different interfacial stress, τ_s values of 0.0649, 0.324, and 0.649 μPa m.

Fig. 2. The particle diameter, as a function of (A) time, and (B) pH, and ζ-potential (C) of WPI samples (▲, heat-denatured; ●, hydrophobised; ■, erythritol-added hydrophobised) during acidification with glucono δ-lactone (GDL) at 37 °C. The heat-denatured and hydrophobised WPI samples were gelled by the addition of GDL at a level of 5 and 20 mg mL^{-1}, respectively. The arrow specifies the onset of protein particles growth in the hydrophobised WPI solution as pH decreases. Error bars represent standard deviation.

Fig. 3. Evolution of the storage modulus (G') of whey protein isolate (WPI) solutions during acidification with glucono δ-lactone (GDL) for (A) up to 150 min and (B) over 1500 min. Symbols in panel A are: ▲, ◆, and ×, heat-denatured WPI at 5, 10 and 20 mg GDL mL^{-1}, respectively; ●, ■ and ●, hydrophobised WPI, erythritol-added hydrophobised WPI and emulsion, respectively, at 20 mg GDL mL^{-1} (error bars represent standard deviation). Symbols in panel B are: ◇ and ×, heat-denatured WPI at 10 and 20 mg GDL mL^{-1}, respectively.

Fig. 4. Mean dynamic moduli of different whey protein isolate (WPI) samples: ▲ and △, heat-denatured WPI; ● and ○, erythritol-free hydrophobised WPI; ◆ and ◇, erythritol-added hydrophobised WPI (diamond); ■ and □, alginate-in-erythritol-added hydrophobised emulsion. Solid symbols indicate storage modulus (G') and the hollow symbols indicate loss modulus (G").

Fig. 5. CLSM images of acid-induced WPI gels and alginate-in-WPI emulsion gel: A, heat-denatured WPI; B, hydrophobised WPI; C, erythritol-added hydrophobised WPI; D, alginate-in-erythritol-added hydrophobised WPI. Panel E presents the results of droplet size analysis of the emulsion gel.

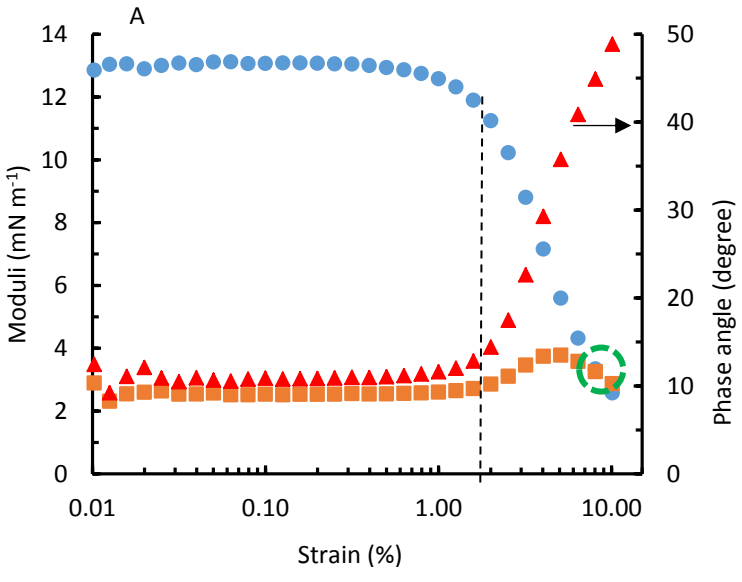
A
Moduli (mN m-1)
Phase angle (degree)
Strain (%)
0.01
0.10
1.00
10.00

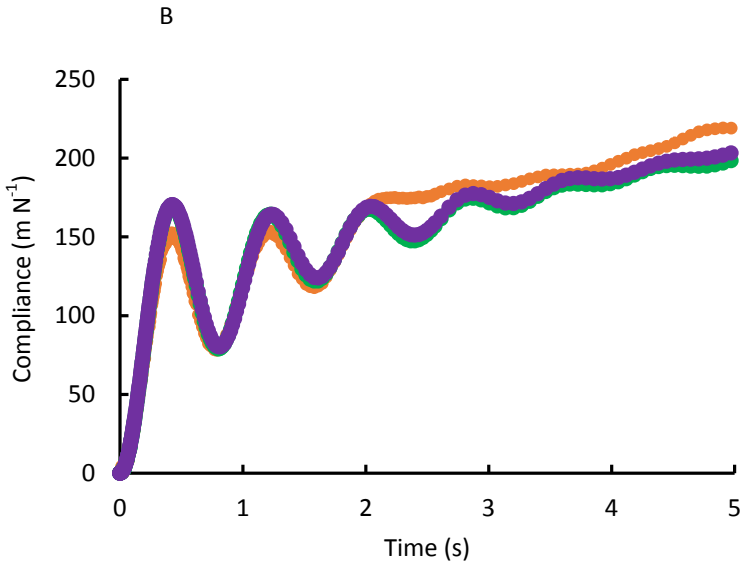
B
Compliance (m N-1)
Time (s)

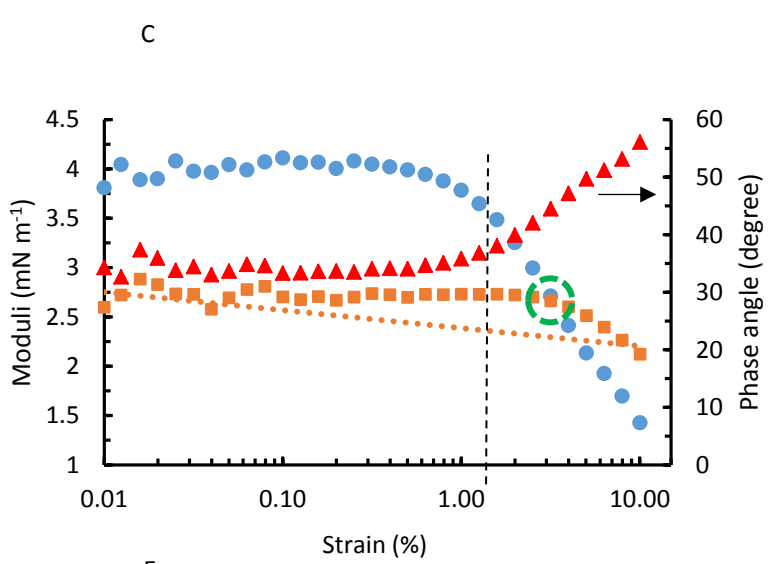
C
Moduli (mN m-1)
Phase angle (degree)
Strain (%)
0.01
0.10
1.00
10.00

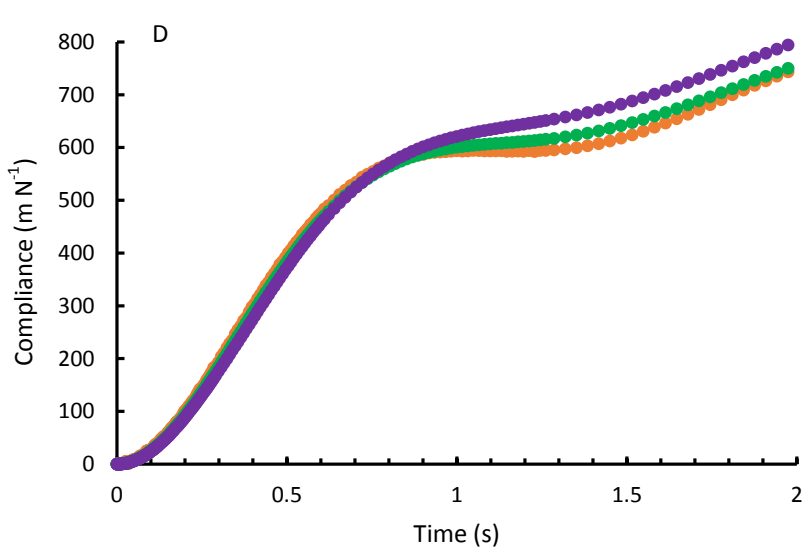
D
Compliance (m N-1)
Time (s)

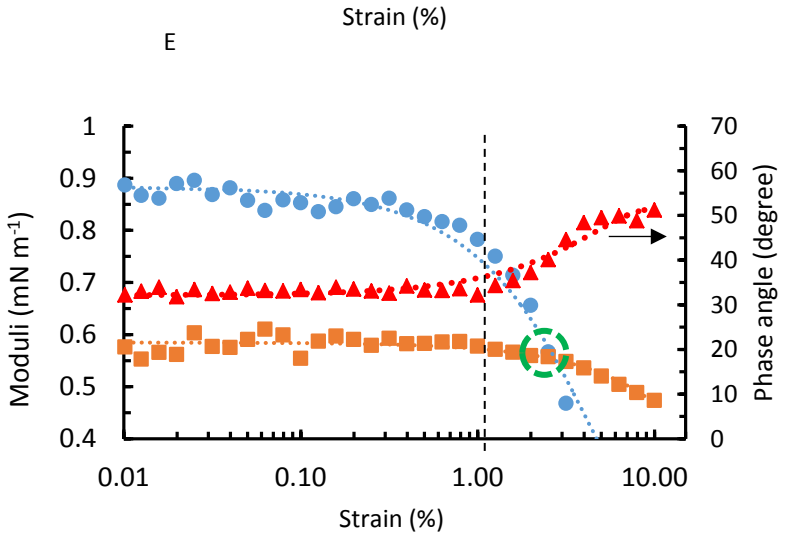
E
Moduli (mN m-1)
Phase angle (degree)
Strain (%)
0.01
0.10
1.00
10.00

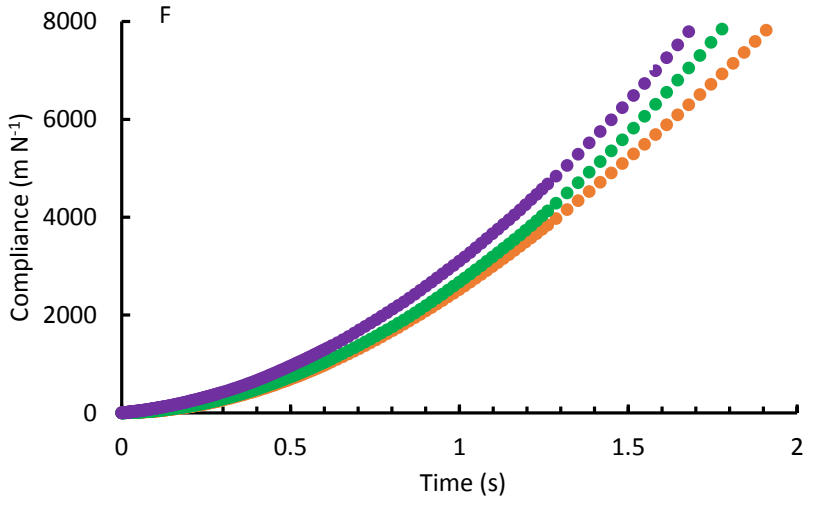
F
Compliance (m N-1)
Time (s)

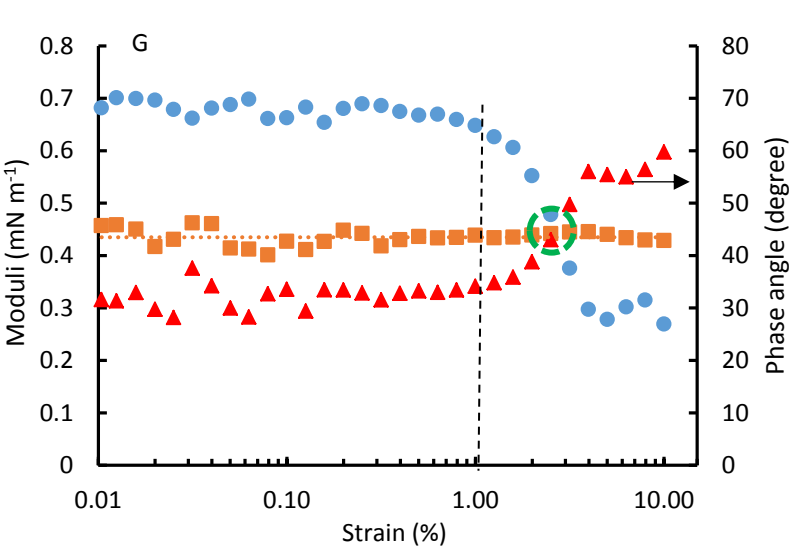
G
Moduli (mN m-1)
Phase angle (degree)
Strain (%)
0.01
0.10
1.00
10.00

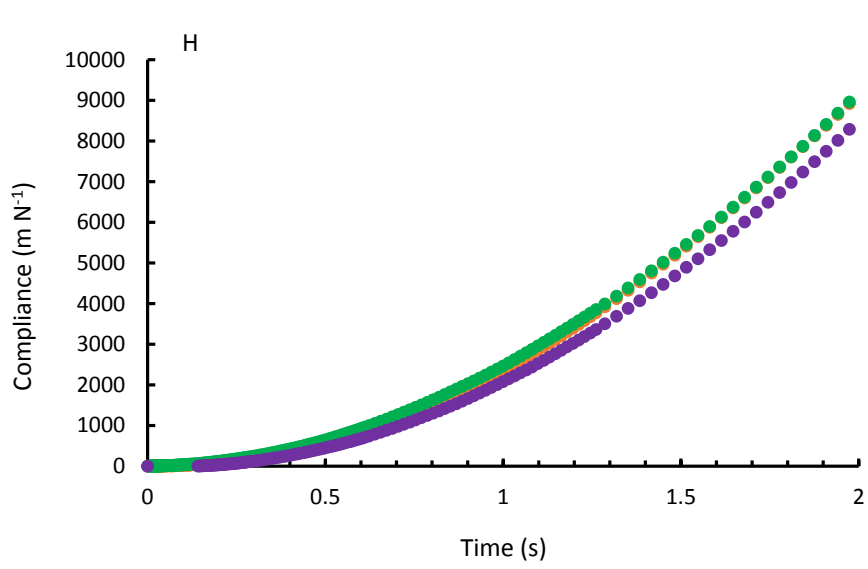
H
Compliance (m N-1)
Time (s)

Figure 1

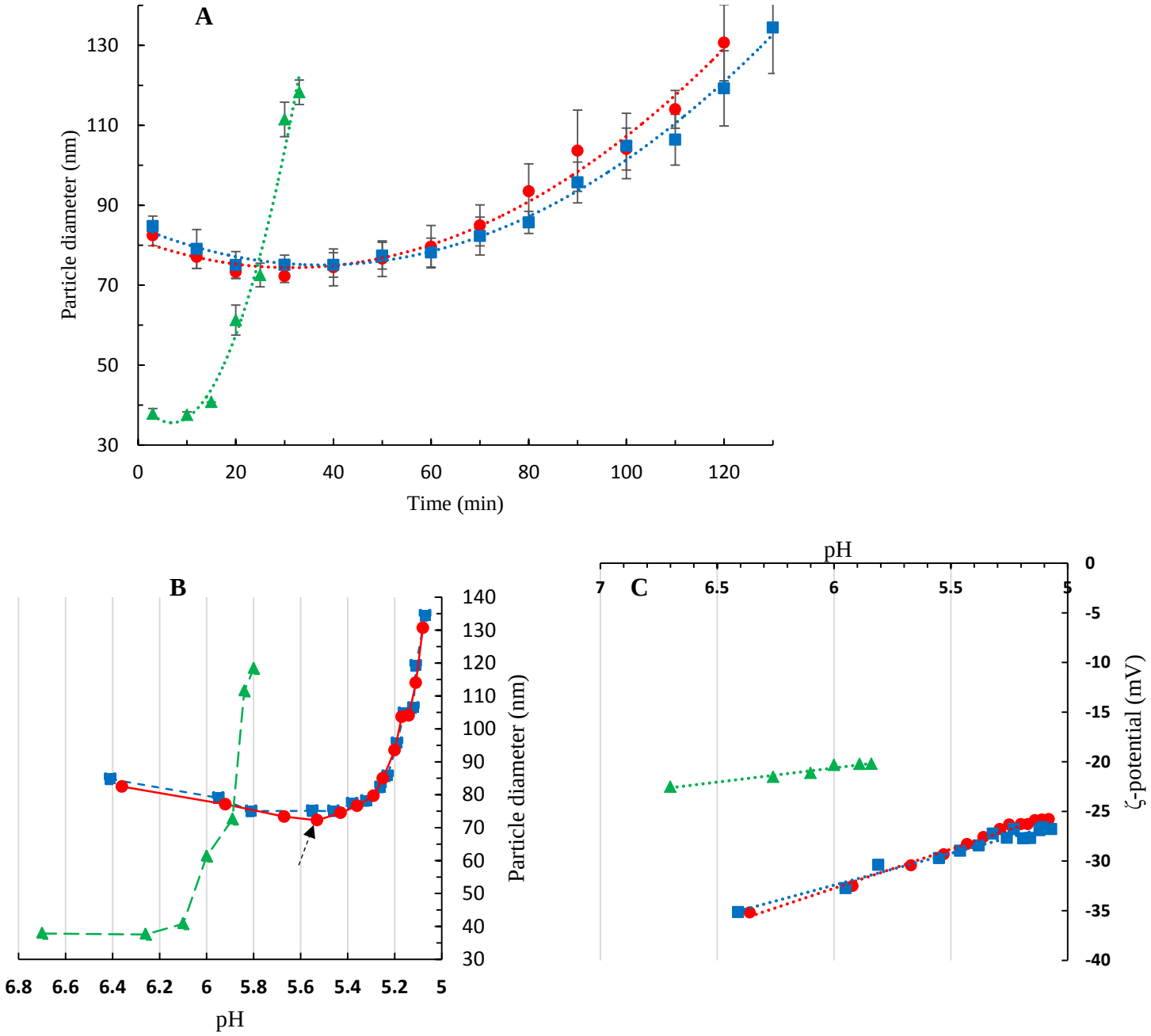
A
Particle diameter (nm)
Time (min)
B
Particle diameter (nm)
pH
C
pH
ζ-potential (mV)

Figure 2

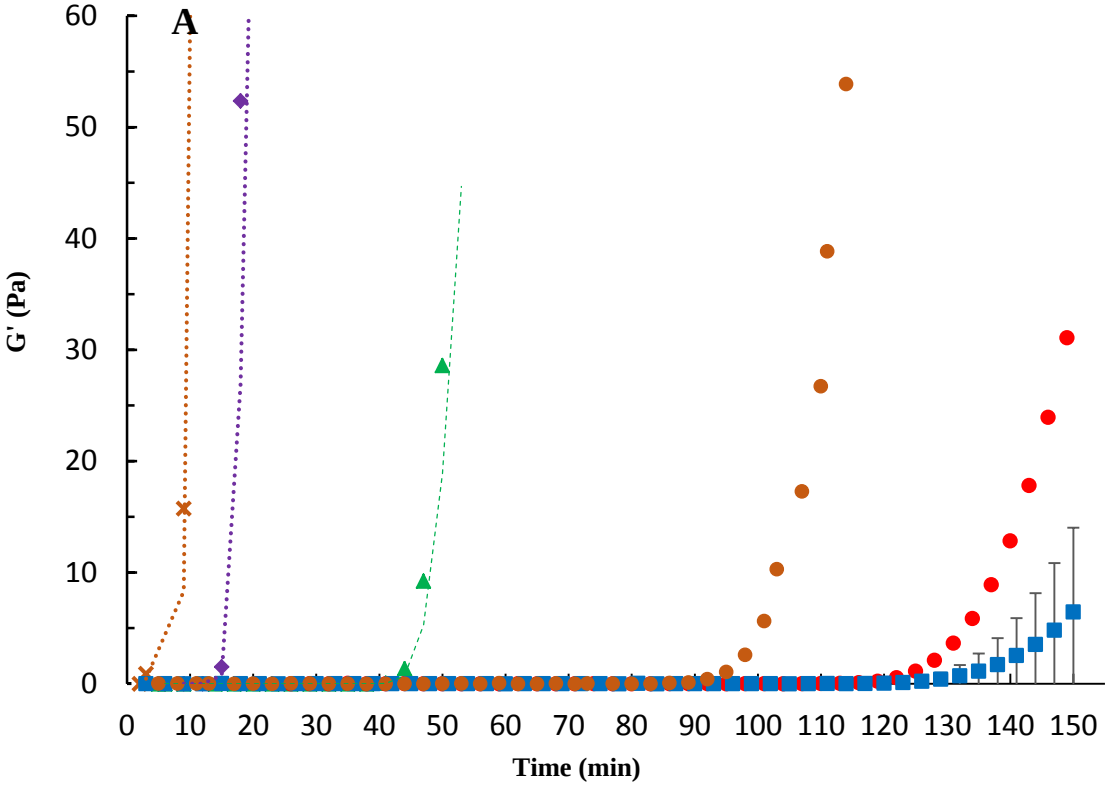
A
G' (Pa)
Time (min)
0
10
20
30
40
50
60
70
80
90
100
110
120
130
140
150

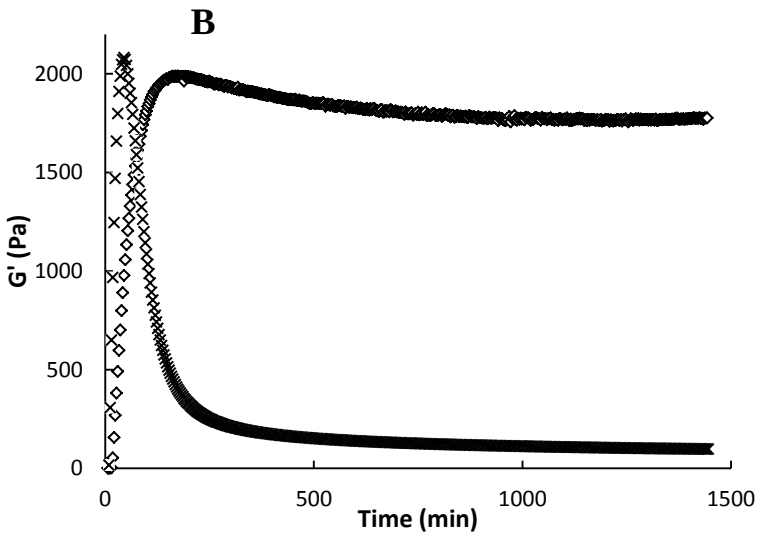
B
G' (Pa)
Time (min)
0
500
1000
1500
2000

Figure 3

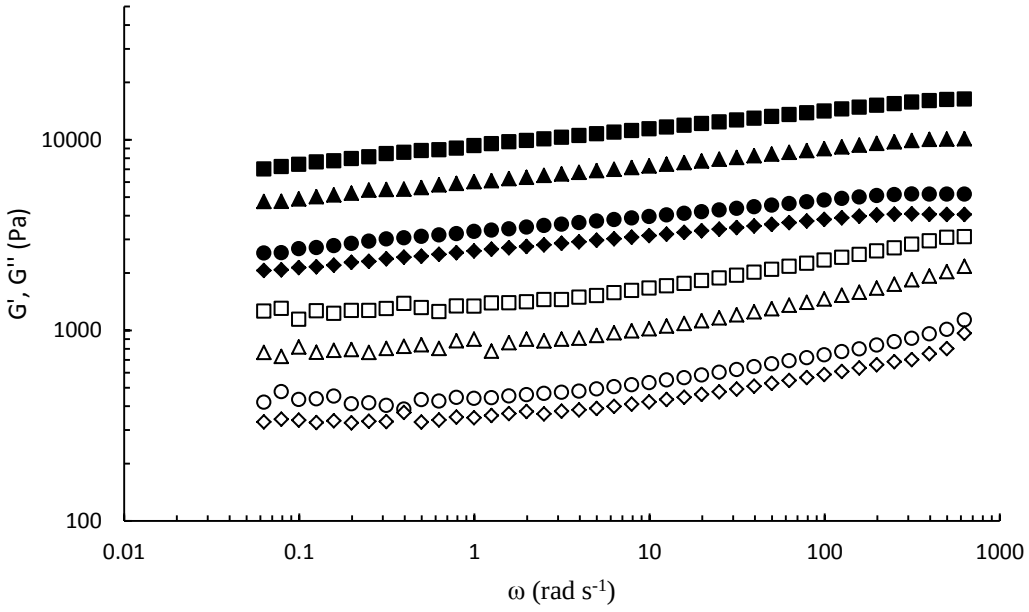

Figure 4

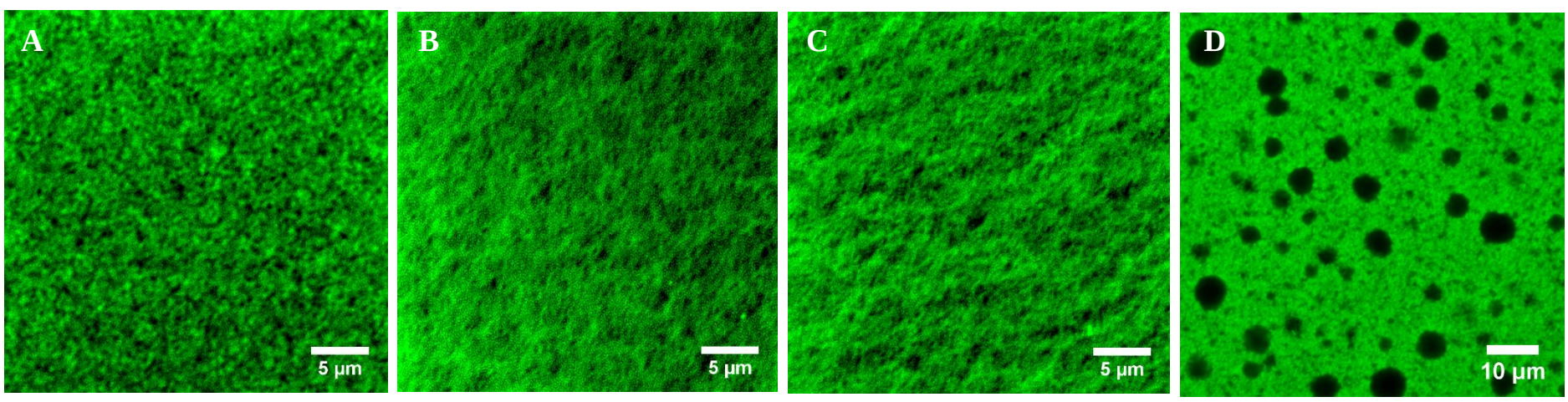
A
5 µm
B
5 µm
C
5 µm
D
10 µm

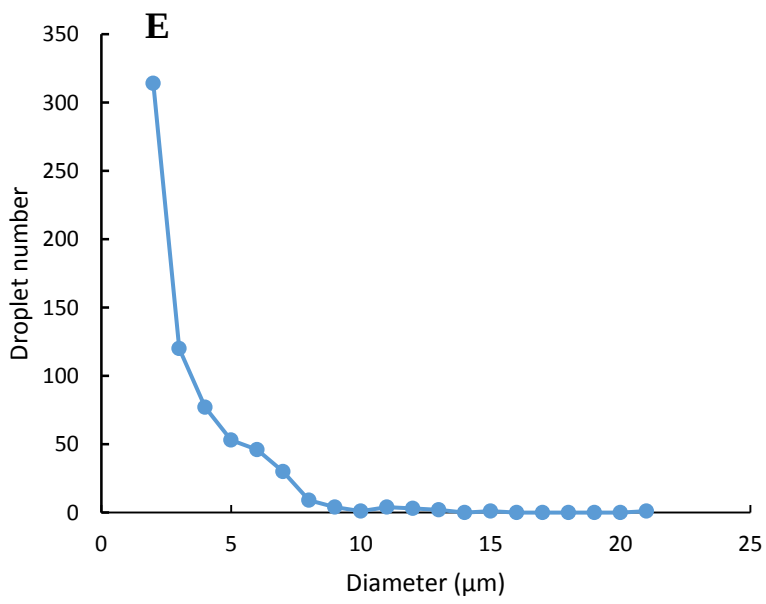
E
Droplet number
Diameter (µm)
0
50
100
150
200
250
300
350
0
5
10
15
20
25

Figure 5

Table 1

Interfacial properties of whey protein isolate (WPI) samples. [a]

Interface	G_s' (mN m^{-1})	δ_l (°)	τ_f (μN m^{-1})	γ_f (%)
Native WPI-air	12.95^{a} ± 0.36	10.9^{b} ± 0.6	3.8	8.0
Heat-denatured WPI-air	4.40^{b} ± 1.3	30.3^{a} ±2.8	1.2	3.1
Hydrophobised WPI-air	0.86^{c} ±0.13	30.9^{a} ±2.7	0.2	2.6
Erythritol-added hydrophobised WPI-air	0.63^{c} ± 0.11	30.5^{a} ±2.1	0.2	2.6

[a] Abbreviations are: G_s', storage modulus in the linear viscoelastic region; δ_l, phase-shift angle in the linear viscoelastic region; τ_f, flow stress; γ_f, flow strain of the interfacial layer. The τ_f and γ_f values were acquired from Fig. 1, which shows typical curves of the strain sweep test at the liquid-air interface of different WPI samples; means with different superscript letters within a column differ significantly ($P < 0.05$).